

Measurements of the branching fractions for J/ψ and $\psi' \rightarrow \Lambda \bar{\Lambda} \pi^0$ and $\Lambda \bar{\Lambda} \eta$

M. Ablikim¹, M. N. Achasov⁶, O. Albayrak³, D. J. Ambrose³⁹, F. F. An¹, Q. An⁴⁰, J. Z. Bai¹,
Y. Ban²⁶, J. Becker², J. V. Bennett¹⁶, M. Bertani^{17A}, J. M. Bian³⁸, E. Boger^{19,a}, O. Bondarenko²⁰,
I. Boyko¹⁹, R. A. Briere³, V. Bytev¹⁹, X. Cai¹, O. Cakir^{34A}, A. Calcaterra^{17A}, G. F. Cao¹,
S. A. Cetin^{34B}, J. F. Chang¹, G. Chelkov^{19,a}, G. Chen¹, H. S. Chen¹, J. C. Chen¹, M. L. Chen¹,
S. J. Chen²⁴, X. Chen²⁶, Y. B. Chen¹, H. P. Cheng¹⁴, Y. P. Chu¹, D. Cronin-Hennessy³⁸,
H. L. Dai¹, J. P. Dai¹, D. Dedovich¹⁹, Z. Y. Deng¹, A. Denig¹⁸, I. Denysenko^{19,b},
M. Destefanis^{43A,43C}, W. M. Ding²⁸, Y. Ding²², L. Y. Dong¹, M. Y. Dong¹, S. X. Du⁴⁶,
J. Fang¹, S. S. Fang¹, L. Fava^{43B,43C}, C. Q. Feng⁴⁰, R. B. Ferrolì^{17A}, P. Friedel², C. D. Fu¹,
Y. Gao³³, C. Geng⁴⁰, K. Goetzen⁷, W. X. Gong¹, W. Gradl¹⁸, M. Greco^{43A,43C}, M. H. Gu¹,
Y. T. Gu⁹, Y. H. Guan³⁶, A. Q. Guo²⁵, L. B. Guo²³, T. Guo²³, Y. P. Guo²⁵, Y. L. Han¹,
F. A. Harris³⁷, K. L. He¹, M. He¹, Z. Y. He²⁵, T. Held², Y. K. Heng¹, Z. L. Hou¹, C. Hu²³,
H. M. Hu¹, J. F. Hu³⁵, T. Hu¹, G. M. Huang⁴, G. S. Huang⁴⁰, J. S. Huang¹², L. Huang¹,
X. T. Huang²⁸, Y. Huang²⁴, Y. P. Huang¹, T. Hussain⁴², C. S. Ji⁴⁰, Q. Ji¹, Q. P. Ji²⁵, X. B. Ji¹,
X. L. Ji¹, L. L. Jiang¹, X. S. Jiang¹, J. B. Jiao²⁸, Z. Jiao¹⁴, D. P. Jin¹, S. Jin¹, F. F. Jing³³,
N. Kalantar-Nayestanaki²⁰, M. Kavatsyuk²⁰, B. Kopf², M. Kornicer³⁷, W. Kuehn³⁵, W. Lai¹,
J. S. Lange³⁵, M. Leyhe², C. H. Li¹, Cheng Li⁴⁰, Cui Li⁴⁰, D. M. Li⁴⁶, F. Li¹, G. Li¹, H. B. Li¹,
J. C. Li¹, K. Li¹⁰, Lei Li¹, Q. J. Li¹, S. L. Li¹, W. D. Li¹, W. G. Li¹, X. L. Li²⁸, X. N. Li¹,
X. Q. Li²⁵, X. R. Li²⁷, Z. B. Li³², H. Liang⁴⁰, Y. F. Liang³⁰, Y. T. Liang³⁵, G. R. Liao³³,
X. T. Liao¹, D. Lin¹¹, B. J. Liu¹, C. L. Liu³, C. X. Liu¹, F. H. Liu²⁹, Fang Liu¹, Feng Liu⁴,
H. Liu¹, H. B. Liu⁹, H. H. Liu¹³, H. M. Liu¹, H. W. Liu¹, J. P. Liu⁴⁴, K. Liu³³, K. Y. Liu²²,
Kai Liu³⁶, P. L. Liu²⁸, Q. Liu³⁶, S. B. Liu⁴⁰, X. Liu²¹, Y. B. Liu²⁵, Z. A. Liu¹, Zhiqiang Liu¹,
Zhiqing Liu¹, H. Loehner²⁰, G. R. Lu¹², H. J. Lu¹⁴, J. G. Lu¹, Q. W. Lu²⁹, X. R. Lu³⁶, Y. P. Lu¹,
C. L. Luo²³, M. X. Luo⁴⁵, T. Luo³⁷, X. L. Luo¹, M. Lv¹, C. L. Ma³⁶, F. C. Ma²², H. L. Ma¹,
Q. M. Ma¹, S. Ma¹, T. Ma¹, X. Y. Ma¹, F. E. Maas¹¹, M. Maggiora^{43A,43C}, Q. A. Malik⁴²,
Y. J. Mao²⁶, Z. P. Mao¹, J. G. Messchendorp²⁰, J. Min¹, T. J. Min¹, R. E. Mitchell¹⁶, X. H. Mo¹,
C. Morales Morales¹¹, N. Yu. Muchnoi⁶, H. Muramatsu³⁹, Y. Nefedov¹⁹, C. Nicholson³⁶,
I. B. Nikolaev⁶, Z. Ning¹, S. L. Olsen²⁷, Q. Ouyang¹, S. Pacetti^{17B}, J. W. Park²⁷, M. Pelizaeus²,

H. P. Peng⁴⁰, K. Peters⁷, J. L. Ping²³, R. G. Ping¹, R. Poling³⁸, E. Prencipe¹⁸, M. Qi²⁴, S. Qian¹,
C. F. Qiao³⁶, L. Q. Qin²⁸, X. S. Qin¹, Y. Qin²⁶, Z. H. Qin¹, J. F. Qiu¹, K. H. Rashid⁴², G. Rong¹,
X. D. Ruan⁹, A. Sarantsev^{19,c}, B. D. Schaefer¹⁶, M. Shao⁴⁰, C. P. Shen^{37,d}, X. Y. Shen¹,
H. Y. Sheng¹, M. R. Shepherd¹⁶, X. Y. Song¹, S. Spataro^{43A,43C}, B. Spruck³⁵, D. H. Sun¹,
G. X. Sun¹, J. F. Sun¹², S. S. Sun¹, Y. J. Sun⁴⁰, Y. Z. Sun¹, Z. J. Sun¹, Z. T. Sun⁴⁰, C. J. Tang³⁰,
X. Tang¹, I. Tapan^{34C}, E. H. Thorndike³⁹, D. Toth³⁸, M. Ullrich³⁵, G. S. Varner³⁷, B. Q. Wang²⁶,
D. Wang²⁶, D. Y. Wang²⁶, K. Wang¹, L. L. Wang¹, L. S. Wang¹, M. Wang²⁸, P. Wang¹,
P. L. Wang¹, Q. J. Wang¹, S. G. Wang²⁶, X. F. Wang³³, X. L. Wang⁴⁰, Y. F. Wang¹, Z. Wang¹,
Z. G. Wang¹, Z. Y. Wang¹, D. H. Wei⁸, J. B. Wei²⁶, P. Weidenkaff¹⁸, Q. G. Wen⁴⁰, S. P. Wen¹,
M. Werner³⁵, U. Wiedner², L. H. Wu¹, N. Wu¹, S. X. Wu⁴⁰, W. Wu²⁵, Z. Wu¹, L. G. Xia³³,
Y. X. Xia¹⁵, Z. J. Xiao²³, Y. G. Xie¹, Q. L. Xiu¹, G. F. Xu¹, G. M. Xu²⁶, Q. J. Xu¹⁰, Q. N. Xu³⁶,
X. P. Xu³¹, Z. R. Xu⁴⁰, F. Xue⁴, Z. Xue¹, L. Yan⁴⁰, W. B. Yan⁴⁰, Y. H. Yan¹⁵, H. X. Yang¹,
Y. Yang⁴, Y. X. Yang⁸, H. Ye¹, M. Ye¹, M. H. Ye⁵, B. X. Yu¹, C. X. Yu²⁵, H. W. Yu²⁶, J. S. Yu²¹,
S. P. Yu²⁸, C. Z. Yuan¹, Y. Yuan¹, A. A. Zafar⁴², A. Zallo^{17A}, Y. Zeng¹⁵, B. X. Zhang¹,
B. Y. Zhang¹, C. Zhang²⁴, C. C. Zhang¹, D. H. Zhang¹, H. H. Zhang³², H. Y. Zhang¹,
J. Q. Zhang¹, J. W. Zhang¹, J. Y. Zhang¹, J. Z. Zhang¹, LiLi Zhang¹⁵, R. Zhang³⁶, S. H. Zhang¹,
X. J. Zhang¹, X. Y. Zhang²⁸, Y. Zhang¹, Y. H. Zhang¹, Z. P. Zhang⁴⁰, Z. Y. Zhang⁴⁴,
Zhenghao Zhang⁴, G. Zhao¹, H. S. Zhao¹, J. W. Zhao¹, K. X. Zhao²³, Lei Zhao⁴⁰,
Ling Zhao¹, M. G. Zhao²⁵, Q. Zhao¹, Q. Z. Zhao⁹, S. J. Zhao⁴⁶, T. C. Zhao¹, Y. B. Zhao¹,
Z. G. Zhao⁴⁰, A. Zhemchugov^{19,a}, B. Zheng⁴¹, J. P. Zheng¹, Y. H. Zheng³⁶, B. Zhong²³,
Z. Zhong⁹, L. Zhou¹, X. K. Zhou³⁶, X. R. Zhou⁴⁰, C. Zhu¹, K. Zhu¹, K. J. Zhu¹, S. H. Zhu¹,
X. L. Zhu³³, Y. C. Zhu⁴⁰, Y. M. Zhu²⁵, Y. S. Zhu¹, Z. A. Zhu¹, J. Zhuang¹, B. S. Zou¹, J. H. Zou¹

(BESIII Collaboration)

¹ *Institute of High Energy Physics, Beijing 100049, People's Republic of China*

² *Bochum Ruhr-University, D-44780 Bochum, Germany*

³ *Carnegie Mellon University, Pittsburgh, Pennsylvania 15213, USA*

⁴ *Central China Normal University, Wuhan 430079, People's Republic of China*

⁵ *China Center of Advanced Science and Technology, Beijing 100190, People's Republic of China*

⁶ *G.I. Budker Institute of Nuclear Physics SB RAS (BINP), Novosibirsk 630090, Russia*

⁷ *GSI Helmholtzcentre for Heavy Ion Research GmbH, D-64291 Darmstadt, Germany*

- ⁸ *Guangxi Normal University, Guilin 541004, People's Republic of China*
- ⁹ *GuangXi University, Nanning 530004, People's Republic of China*
- ¹⁰ *Hangzhou Normal University, Hangzhou 310036, People's Republic of China*
- ¹¹ *Helmholtz Institute Mainz, Johann-Joachim-Becher-Weg 45, D-55099 Mainz, Germany*
- ¹² *Henan Normal University, Xinxiang 453007, People's Republic of China*
- ¹³ *Henan University of Science and Technology, Luoyang 471003, People's Republic of China*
- ¹⁴ *Huangshan College, Huangshan 245000, People's Republic of China*
- ¹⁵ *Hunan University, Changsha 410082, People's Republic of China*
- ¹⁶ *Indiana University, Bloomington, Indiana 47405, USA*
- ¹⁷ *(A)INFN Laboratori Nazionali di Frascati, I-00044, Frascati, Italy; (B)INFN and University of Perugia, I-06100, Perugia, Italy*
- ¹⁸ *Johannes Gutenberg University of Mainz, Johann-Joachim-Becher-Weg 45, D-55099 Mainz, Germany*
- ¹⁹ *Joint Institute for Nuclear Research, 141980 Dubna, Moscow region, Russia*
- ²⁰ *KVI, University of Groningen, NL-9747 AA Groningen, The Netherlands*
- ²¹ *Lanzhou University, Lanzhou 730000, People's Republic of China*
- ²² *Liaoning University, Shenyang 110036, People's Republic of China*
- ²³ *Nanjing Normal University, Nanjing 210023, People's Republic of China*
- ²⁴ *Nanjing University, Nanjing 210093, People's Republic of China*
- ²⁵ *Nankai University, Tianjin 300071, People's Republic of China*
- ²⁶ *Peking University, Beijing 100871, People's Republic of China*
- ²⁷ *Seoul National University, Seoul, 151-747 Korea*
- ²⁸ *Shandong University, Jinan 250100, People's Republic of China*
- ²⁹ *Shanxi University, Taiyuan 030006, People's Republic of China*
- ³⁰ *Sichuan University, Chengdu 610064, People's Republic of China*
- ³¹ *Soochow University, Suzhou 215006, People's Republic of China*
- ³² *Sun Yat-Sen University, Guangzhou 510275, People's Republic of China*
- ³³ *Tsinghua University, Beijing 100084, People's Republic of China*
- ³⁴ *(A)Ankara University, Dogol Caddesi, 06100 Tandogan, Ankara, Turkey; (B)Dogus University, 34722 Istanbul, Turkey; (C)Uludag University, 16059 Bursa, Turkey*

³⁵ *Universitaet Giessen, D-35392 Giessen, Germany*

³⁶ *University of Chinese Academy of Sciences, Beijing 100049, People's Republic of China*

³⁷ *University of Hawaii, Honolulu, Hawaii 96822, USA*

³⁸ *University of Minnesota, Minneapolis, Minnesota 55455, USA*

³⁹ *University of Rochester, Rochester, New York 14627, USA*

⁴⁰ *University of Science and Technology of China, Hefei 230026, People's Republic of China*

⁴¹ *University of South China, Hengyang 421001, People's Republic of China*

⁴² *University of the Punjab, Lahore-54590, Pakistan*

⁴³ (A)*University of Turin, I-10125, Turin, Italy*; (B)*University of Eastern Piedmont, I-15121, Alessandria, Italy*; (C)*INFN, I-10125, Turin, Italy*

⁴⁴ *Wuhan University, Wuhan 430072, People's Republic of China*

⁴⁵ *Zhejiang University, Hangzhou 310027, People's Republic of China*

⁴⁶ *Zhengzhou University, Zhengzhou 450001, People's Republic of China*

^a *Also at the Moscow Institute of Physics and Technology, Moscow 141700, Russia*

^b *On leave from the Bogolyubov Institute for Theoretical Physics, Kiev 03680, Ukraine*

^c *Also at the PNPI, Gatchina 188300, Russia*

^d *Present address: Nagoya University, Nagoya 464-8601, Japan*

Abstract

We report on a study of the isospin-violating and conserving decays of the J/ψ and ψ' charmonium state to $\Lambda\bar{\Lambda}\pi^0$ and $\Lambda\bar{\Lambda}\eta$, respectively. The data are based on 225 million J/ψ and 106 million ψ' events that were collected with the BESIII detector. The most accurate measurement of the branching fraction of the isospin-violating process $J/\psi \rightarrow \Lambda\bar{\Lambda}\pi^0$ is obtained, and the isospin-conserving processes $J/\psi \rightarrow \Lambda\bar{\Lambda}\eta$ and $\psi' \rightarrow \Lambda\bar{\Lambda}\eta$ are observed for the first time. The branching fractions are measured to be $\mathcal{B}(J/\psi \rightarrow \Lambda\bar{\Lambda}\pi^0) = (3.78 \pm 0.27_{\text{stat}}) \pm 0.29_{\text{sys}} \times 10^{-5}$, $\mathcal{B}(J/\psi \rightarrow \Lambda\bar{\Lambda}\eta) = (15.7 \pm 0.79_{\text{stat}} \pm 1.52_{\text{sys}}) \times 10^{-5}$ and $\mathcal{B}(\psi' \rightarrow \Lambda\bar{\Lambda}\eta) = (2.47 \pm 0.34_{\text{stat}} \pm 0.19_{\text{sys}}) \times 10^{-5}$. No significant signal events are observed for $\psi' \rightarrow \Lambda\bar{\Lambda}\pi^0$ decay resulting in an upper limit of the branching fraction of $\mathcal{B}(\psi' \rightarrow \Lambda\bar{\Lambda}\pi^0) < 0.29 \times 10^{-5}$ at the 90% confidence level. The two-body decay of $J/\psi \rightarrow \Sigma(1385)^0\bar{\Lambda} + c.c.$ is searched for, and the upper limit is $\mathcal{B}(J/\psi \rightarrow \Sigma(1385)^0\bar{\Lambda} + c.c.) < 0.81 \times 10^{-5}$ at the 90% confidence level.

PACS numbers: 13.25.Gv, 12.38.Qk, 14.20.Gk, 14.40.Cs

I. INTRODUCTION

The charmonium vector meson, J/ψ , is usually interpreted as an SU(3) singlet $c\bar{c}$ bound states with an isospin $I=0$. Systematic measurements of its decay rates into final states that are isospin violating are of particular interest, since these results will provide a sensitive probe to study symmetry-breaking effects in a controlled environment. In this paper, we present a systematic study of isospin-conserving and violating decays of charmonium vector mesons into baryonic decays accompanied by a light pseudoscalar meson, namely $J/\psi(\psi') \rightarrow \Lambda\bar{\Lambda}\eta$ and $J/\psi(\psi') \rightarrow \Lambda\bar{\Lambda}\pi^0$, respectively.

This work is for a large part motivated by a controversial observation that was made in the past while studying the baryonic decay of the J/ψ . Surprisingly, the average branching fraction of the isospin violating decay of $J/\psi \rightarrow \Lambda\bar{\Lambda}\pi^0$ measured by DM2 [1] and by BES I [2] was determined to be $\mathcal{B}(J/\psi \rightarrow \Lambda\bar{\Lambda}\pi^0) = (2.2 \pm 0.6) \times 10^{-4}$, while the isospin conserving decay mode $J/\psi \rightarrow \Lambda\bar{\Lambda}\eta$ was not reported by either experiment. In 2007, the decays of J/ψ and ψ' to the final states with a $\Lambda\bar{\Lambda}$ pair plus a neutral pseudoscalar meson were studied using 58 million J/ψ and 14 million ψ' events collected with the BES II detector [3]. The new measurement suggested that the two previous studies of $J/\psi \rightarrow \Lambda\bar{\Lambda}\pi^0$ may have overlooked the sizable background contribution from $J/\psi \rightarrow \Sigma^0\pi^0\bar{\Lambda} + c.c..$ The BES II experiment removed this type of background contribution and only a few statistically insignificant $J/\psi \rightarrow \Lambda\bar{\Lambda}\pi^0$ signal events remained, resulting in an upper limit of $\mathcal{B}(J/\psi \rightarrow \Lambda\bar{\Lambda}\pi^0) < 0.64 \times 10^{-4}$. Moreover, the isospin conserving decay mode, $J/\psi \rightarrow \Lambda\bar{\Lambda}\eta$, was observed for the first time with a significance of 4.8σ . However, signal events of the channels $\psi' \rightarrow \Lambda\bar{\Lambda}\pi^0$ and $\psi' \rightarrow \Lambda\bar{\Lambda}\eta$ were not observed by BES II, and resulted in upper limits of $\mathcal{B}(\psi' \rightarrow \Lambda\bar{\Lambda}\pi^0) < 4.9 \times 10^{-5}$ and $\mathcal{B}(\psi' \rightarrow \Lambda\bar{\Lambda}\eta) < 1.2 \times 10^{-4}$.

In 2009, BES III collected 225 million J/ψ [4] and 106 million ψ' [5] events. These samples provide a unique opportunity to revisit these isospin conserving and violating decays with improved sensitivity to confirm the previous observations in J/ψ decays with BES II. The ambition is to investigate as well the same final states in ψ' decays with the new record in statistics, and look for possible anomalies. A measurement of these branching fractions would be a test of the “12%” rule [6]. The data allow in addition a search for the two-body decays $J/\psi \rightarrow \Sigma(1385)^0\bar{\Lambda} + c.c..$

II. EXPERIMENTAL DETAILS

BEPCII is a double-ring e^+e^- collider that has reached a peak luminosity of about $0.6 \times 10^{33} \text{ cm}^{-2}\text{s}^{-1}$ at the center of mass energy of 3.77 GeV. The cylindrical core of the BESIII detector consists of a helium-based main drift chamber (MDC), a plastic scintillator time-of-flight system (TOF), and a CsI(Tl) electromagnetic calorimeter (EMC), which are all enclosed in a superconducting solenoidal magnet providing a 1.0 T magnetic field. The solenoid is supported by an octagonal flux-return yoke with resistive plate counter muon identifier modules interleaved with steel. The acceptance for charged particles and photons is 93% over 4π stereo angle, and the charged-particle momentum and photon energy resolutions at 1 GeV are 0.5% and 2.5%, respectively. The detector is described in more detail in [7].

The optimization of the event selection criteria and the estimates of physics background sources are performed through Monte Carlo (MC) simulations. The BESIII detector is modeled with the GEANT4 toolkit [8, 9]. Signal events are generated according to a uniform phase-space distribution. Inclusive J/ψ and ψ' decays are simulated with the KKMC [10] generator. Known decays are modeled by the EVTGEN [11] generator according to the branching fractions provided by the Particle Data Group (PDG) [12], and the remaining unknown decay modes are generated with the LUNDCHARM model [13].

III. EVENT SELECTION

The decay channels investigated in this paper are $J/\psi (\psi') \rightarrow \Lambda \bar{\Lambda} \pi^0$ and $J/\psi (\psi') \rightarrow \Lambda \bar{\Lambda} \eta$. The final states include Λ , $\bar{\Lambda}$ and one neutral pseudoscalar meson (π^0 or η), where Λ ($\bar{\Lambda}$) decays to $\pi^- p$ ($\pi^+ \bar{p}$), while the π^0 and η decay to $\gamma\gamma$. Candidate events are required to satisfy the following common selection criteria:

1. Only events with at least two positively charged and two negatively charged tracks are kept. No requirements are made on the impact parameters of the charged tracks as the tracks are supposed to originate from secondary vertices.
2. The transverse momenta of the proton and anti-proton are required to be larger than 0.2 GeV/ c . Tracks with smaller transverse momenta are removed since the MC simulation fails to describe such extremely soft tracks.

3. Photon candidates are identified from the reconstructed showers in the EMC. Photon energies are required to be larger than 25 MeV in the EMC barrel region ($|\cos\theta| < 0.8$) and larger than 50 MeV in the EMC end-cap ($0.86 < |\cos\theta| < 0.92$). The overlapping showers between the barrel and end-cap ($0.8 < |\cos\theta| < 0.86$) are poorly reconstructed, therefore, excluded from the analysis. In addition, timing requirements are imposed on photon candidates to suppress electronic noise and energy deposits from uncorrelated events.
4. The Λ and $\bar{\Lambda}$ candidates are identified by a reconstruction of decay vertices from pairs of oppositely charged tracks $p\pi^-$ and $\bar{p}\pi^+$ [14]. At least one $p\pi^-$ and one $\bar{p}\pi^+$ candidate are required to pass the Λ ($\bar{\Lambda}$) vertex fit successfully by looping over all the combinations of positive and negative charged tracks. In the case of multiple $\Lambda\bar{\Lambda}$ pair candidates, the one with the minimum value of $(M_{p\pi^-} - M_\Lambda)^2 + (M_{\bar{p}\pi^+} - M_{\bar{\Lambda}})^2$ is chosen, where $M_\Lambda(M_{\bar{\Lambda}})$ is the nominal mass of $\Lambda(\bar{\Lambda})$, obtained from the PDG [12].
5. To further reduce the background and to improve the resolution of the reconstructed particle momenta, candidate signal events are subjected to a four constraint energy-momentum conservation (4C) kinematic fit under the hypothesis of J/ψ (ψ') $\rightarrow \Lambda\bar{\Lambda}\gamma\gamma$. In the case of several combinations due to additional photons, the one with the best χ_{4C}^2 value is chosen. In addition, a selection is made on the χ_{4C}^2 . Its value is determined by optimizing the signal significance $S/\sqrt{S+B}$, where S (B) is the number of signal (background) events in the signal region. This requirement is effective against background with one or several additional photons like J/ψ , $\psi' \rightarrow \Sigma^0\pi^0\bar{\Lambda} + c.c.$ ($\Sigma^0 \rightarrow \gamma\Lambda$) or J/ψ , $\psi' \rightarrow \Lambda\bar{\Lambda} + n\gamma$ ($n \geq 4$) decays (for instance J/ψ , $\psi' \rightarrow \Sigma(1385)^0\bar{\Sigma}(1385)^0$, $\Xi^0\bar{\Xi}^0$, etc.). For $J/\psi \rightarrow \Lambda\bar{\Lambda}\pi^0$, backgrounds are suppressed by requiring $\chi_{4C}^2 < 40$ (see Fig. 1(a)). For $J/\psi \rightarrow \Lambda\bar{\Lambda}\eta$, the requirement is set to $\chi_{4C}^2 < 70$ (see Fig. 1(b)). For $\psi' \rightarrow \Lambda\bar{\Lambda}\pi^0$, due to the peaking background $\psi' \rightarrow \Sigma^0\pi^0\bar{\Lambda} + c.c.$ the χ_{4C}^2 is required to be less than 15 (see Fig. 1(c)). For $\psi' \rightarrow \Lambda\bar{\Lambda}\eta$, we select events with $\chi_{4C}^2 < 40$ (see Fig. 1(d)).

Followed by the common selection criteria, a further background reduction is obtained by applying various mass constraints depending on the channel of interest. To select a clean sample of Λ and $\bar{\Lambda}$ signal events, the invariant masses of $p\pi^-$ and $\bar{p}\pi^+$ are required to be within the mass window of $|M_{p\pi} - M_\Lambda| < 5 \text{ MeV}/c^2$. Here, the invariant mass is reconstructed with improved momenta from the 4C kinematic fit. The mass resolutions of Λ and $\bar{\Lambda}$ are about $1.0 \text{ MeV}/c^2$. For $J/\psi \rightarrow \Lambda\bar{\Lambda}\pi^0$, a mass selection of $|M_{p\pi^0} - 1189.0| > 10 \text{ MeV}/c^2$ is used to exclude background

from $J/\psi \rightarrow \Sigma^+ \pi^- \bar{\Lambda} + c.c.$ ($\Sigma^+ \rightarrow p \pi^0$) which can form a peak near the π^0 mass. The background from $J/\psi \rightarrow \Sigma^0 \bar{\Sigma}^0$ is removed by selecting events with $M_{\Lambda\bar{\Lambda}} < 2.8 \text{ GeV}/c^2$ as shown in Fig. 2(a). For $J/\psi \rightarrow \Lambda \bar{\Lambda} \eta$, a selection of events with $M_{\Lambda\bar{\Lambda}} < 2.6 \text{ GeV}/c^2$ rejects all background contributions from $J/\psi \rightarrow \Sigma^0 \bar{\Sigma}^0$ decays as shown in Fig. 2(b). For $\psi' \rightarrow \Lambda \bar{\Lambda} \pi^0$ and $\psi' \rightarrow \Lambda \bar{\Lambda} \eta$, events must satisfy the condition $|M_{\pi^+\pi^-}^{\text{recoil}} - 3097| > 8 \text{ MeV}/c^2$ to remove the background from $\psi' \rightarrow \pi^+\pi^- J/\psi$ ($J/\psi \rightarrow p\bar{p}\pi^0$ and $p\bar{p}\eta$). The background from $\psi' \rightarrow \gamma\gamma J/\psi$ ($J/\psi \rightarrow \Lambda \bar{\Lambda}$) and $\psi' \rightarrow \Sigma^0 \bar{\Sigma}^0$ is rejected by the requirement $M_{\Lambda\bar{\Lambda}} < 3.08 \text{ GeV}/c^2$. The $\Lambda\bar{\Lambda}$ invariant-mass distributions for data and MC events from $\psi' \rightarrow \Lambda \bar{\Lambda} \pi^0$, $\Lambda \bar{\Lambda} \eta$, and $\Sigma^0 \bar{\Sigma}^0$ are shown in Fig. 3. The scatter plot of $M_{p\pi^-}$ versus $M_{\bar{p}\pi^+}$ after applying all selection criteria is shown in Fig. 4. No visible signal of $\psi' \rightarrow \Lambda \bar{\Lambda} \pi^0$ is observed.

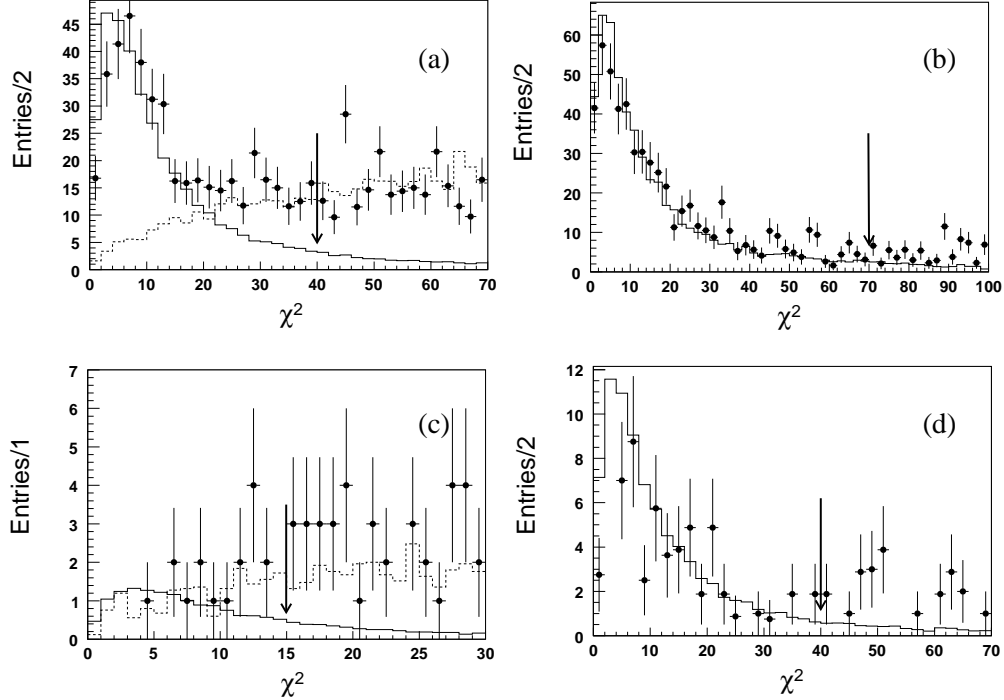


FIG. 1: The χ^2_{4C} distributions of 4C fits. Dots with error bars denote data, and the histograms correspond to the result of MC simulations. (a) $J/\psi \rightarrow \Lambda \bar{\Lambda} \pi^0$. The dashed line is the dominant background distribution from $J/\psi \rightarrow \Sigma^0 \pi^0 \bar{\Lambda} + c.c.$ with MC simulated events, the arrow denotes the selection of $\chi^2_{4C} < 40$. (b) $J/\psi \rightarrow \Lambda \bar{\Lambda} \eta$, the arrow denotes the selection of $\chi^2_{4C} < 70$. (c) $\psi' \rightarrow \Lambda \bar{\Lambda} \pi^0$. The dashed line is the dominant background distribution from $\psi' \rightarrow \Sigma^0 \pi^0 \bar{\Lambda} + c.c.$ with MC simulated events, the arrow denotes the selection of $\chi^2_{4C} < 15$. (d) $\psi' \rightarrow \Lambda \bar{\Lambda} \eta$, and the arrow denotes the selection of $\chi^2_{4C} < 40$.

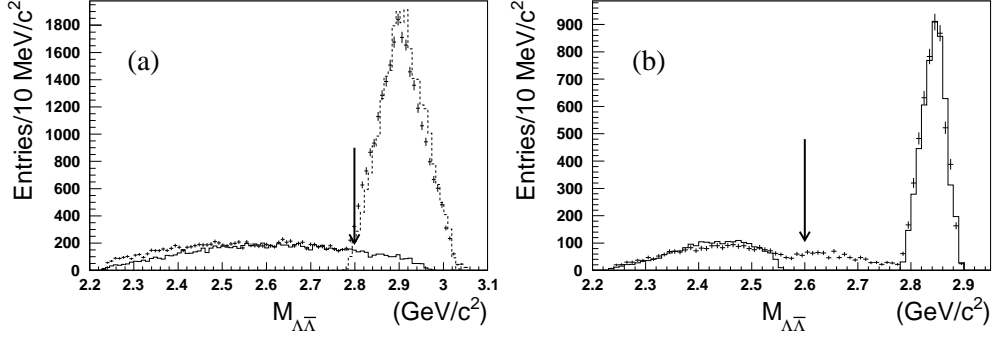


FIG. 2: The $\Lambda\bar{\Lambda}$ invariant-mass, $M_{\Lambda\bar{\Lambda}}$, distributions for $J/\psi \rightarrow \Lambda\bar{\Lambda}\gamma\gamma$ candidates. Dots with errors denote data. The dashed-line shows the result of MC simulated events of $J/\psi \rightarrow \Sigma^0\bar{\Sigma}^0$ which is normalized according to the branching fraction from the PDG. (a) Histogram shows the MC simulated events of $J/\psi \rightarrow \Lambda\bar{\Lambda}\pi^0$, where the arrow denotes the selection of $M_{\Lambda\bar{\Lambda}} < 2.8 \text{ GeV}/c^2$. (b) Histogram shows the MC simulated events of $J/\psi \rightarrow \Lambda\bar{\Lambda}\eta$, and the arrow shows the selection of $M_{\Lambda\bar{\Lambda}} < 2.6 \text{ GeV}/c^2$.

IV. BACKGROUND STUDY

Backgrounds that have the same final states as the signal channels such as $J/\psi, \psi' \rightarrow \Sigma^0\bar{\Sigma}^0, \Sigma^+\pi^-\bar{\Lambda} + c.c.$ are either suppressed to a negligible level or completely removed. Background channels that contain one or more photons than the signal channels like $J/\psi, \psi' \rightarrow \Sigma(1385)^0\bar{\Sigma}(1385)^0, \Xi^0\bar{\Xi}^0$ have very few events passing event selection. The line shape of the peaking background sources, $J/\psi, \psi' \rightarrow \Sigma^0\pi^0\bar{\Lambda} + c.c.$, is used in the fitting procedure to estimate their contributions. The contribution of remaining backgrounds from non- $\Lambda\bar{\Lambda}$ decays including $J/\psi, \psi' \rightarrow \pi^+\pi^-p\bar{p}\pi^0$ (η) is estimated using sideband studies as illustrated in Fig. 4. The square with a width of $10 \text{ MeV}/c^2$ around the nominal mass of the Λ and $\bar{\Lambda}$ is taken as the signal region. The eight squares surrounding the signal region are taken as sideband regions. The area of all the squares is equal. The sum of events in the sideband squares, $\sum N_{\text{sideband region}}$, times a normalization factor f is taken as the background contribution in the signal region. The normalization factor f is defined as

$$f = \frac{N_{\text{signal region}}}{\sum N_{\text{sideband region}}}.$$

The normalization factor is obtained from phase-space MC simulations of $J/\psi (\psi') \rightarrow p\bar{p}\pi^+\pi^-\pi^0$ or $p\bar{p}\pi^+\pi^-\eta$ with $N_{\text{signal region}}$ as the number of MC events in the signal region and $\sum N_{\text{sideband region}}$ as the sum of MC events in the sideband regions.

With 44 pb^{-1} of data collected at a center-of-mass energy of $E_{cm} = 3.65 \text{ GeV}$, the contribution

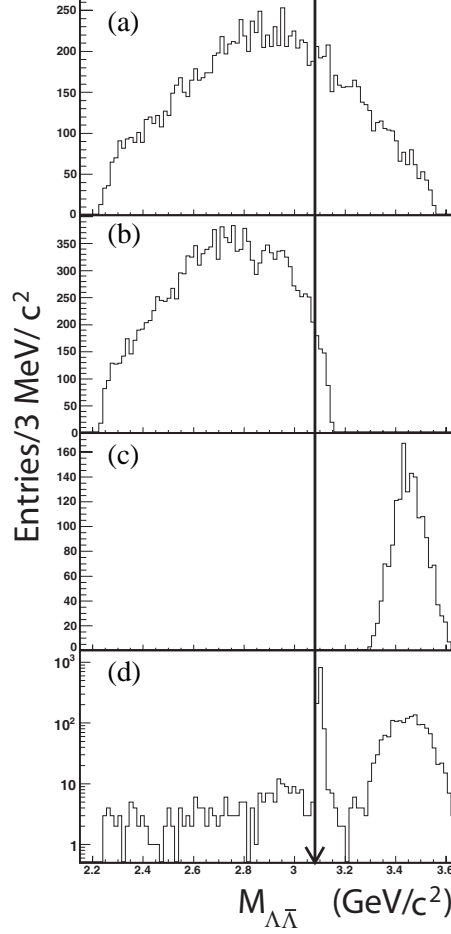


FIG. 3: The $\Lambda\bar{\Lambda}$ invariant-mass, $M_{\Lambda\bar{\Lambda}}$, distributions for $\psi' \rightarrow \Lambda\bar{\Lambda}\gamma\gamma$ candidates. (a) MC simulated events of $\psi' \rightarrow \Lambda\bar{\Lambda}\pi^0$, (b) MC simulated events of $\psi' \rightarrow \Lambda\bar{\Lambda}\eta$, (c) MC simulated events of $\psi' \rightarrow \Sigma^0\bar{\Sigma}^0$, and (d) data. The arrow denotes the selection of $M_{\Lambda\bar{\Lambda}} < 3.08 \text{ GeV}/c^2$. The peak around the J/ψ mass is from the decay of $\psi' \rightarrow \gamma\gamma J/\psi$, $J/\psi \rightarrow \Lambda\bar{\Lambda}$.

from the continuum background is determined. From this data sample, no events survive in the π^0 or η mass region in the two-photon invariant-mass, $M_{\gamma\gamma}$, distribution after applying all selection criteria. Therefore, we neglect this background.

V. SIGNAL YIELDS AND DALITZ ANALYSES

The $\gamma\gamma$ invariant-mass spectra of $J/\psi \rightarrow \Lambda\bar{\Lambda}\pi^0$, $\Lambda\bar{\Lambda}\eta$, $\psi' \rightarrow \Lambda\bar{\Lambda}\pi^0$ and $\Lambda\bar{\Lambda}\eta$ of the remaining events after the previously described signal selection procedure are shown in Fig. 5. A clear π^0

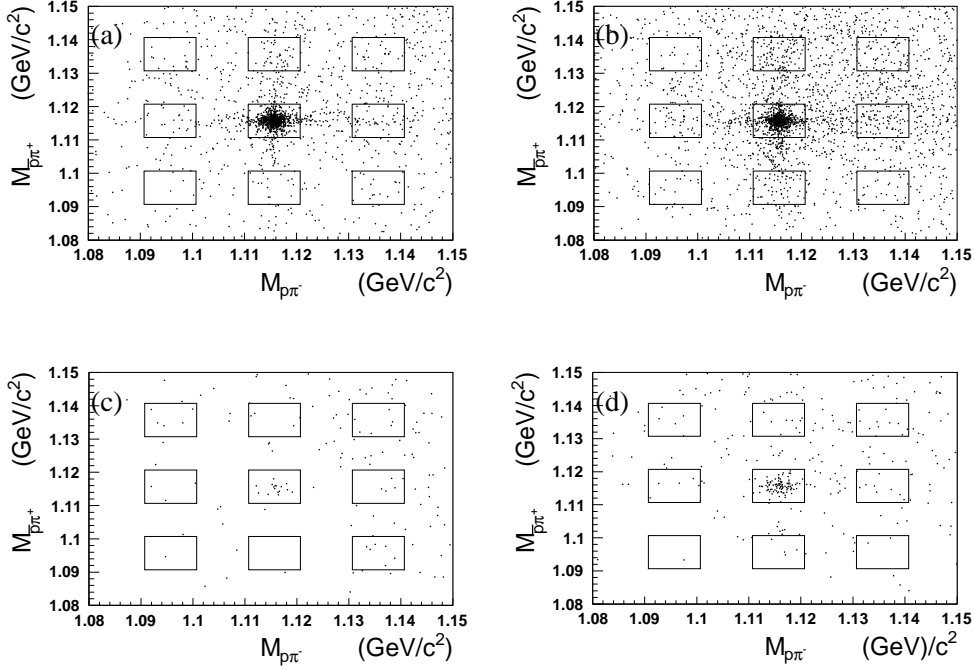


FIG. 4: A scatter plot of $M_{\bar{p}\pi^+}$ versus $M_{p\pi^-}$ for J/ψ and ψ' data. (a) $J/\psi \rightarrow \Lambda \bar{\Lambda} \pi^0$, (b) $J/\psi \rightarrow \Lambda \bar{\Lambda} \eta$, (c) $\psi' \rightarrow \Lambda \bar{\Lambda} \pi^0$, and (d) $\psi' \rightarrow \Lambda \bar{\Lambda} \eta$.

and η signal can be observed in the J/ψ data. The ψ' data set shows a significant η signal, but lacks a pronounced peak near the π^0 mass.

The number of signal events are extracted by fitting the $M_{\gamma\gamma}$ distributions with the parameterized signal shape from MC simulations. For J/ψ (ψ') $\rightarrow \Lambda \bar{\Lambda} \pi^0$, the dominant peaking backgrounds from J/ψ (ψ') $\rightarrow \Sigma^0 \pi^0 \bar{\Lambda} + c.c.$ are estimated by MC simulation. The fit also accounts for background estimates from a normalized sideband analysis. Other background sources are described by a Chebychev polynomial for all channels except $\psi' \rightarrow \Lambda \bar{\Lambda} \pi^0$ where there are too few events surviving. The fit yields 323 ± 23 π^0 events, 454 ± 23 η events in J/ψ data and 60.4 ± 8.4 η events in ψ' data. For $\psi' \rightarrow \Lambda \bar{\Lambda} \pi^0$, the upper limit on N_{π^0} is 9 at the 90% confidence level (C.L.) and is determined with a Bayesian method [15]. For $\psi' \rightarrow \Lambda \bar{\Lambda} \eta$, the change in log likelihood value in the fit with and without the signal function is used to determine the η signal significance, which is estimated to be 10.5σ .

To study the existence of intermediate resonance states in the decay of $J/\psi \rightarrow \Lambda \bar{\Lambda} \pi^0$, $J/\psi \rightarrow \Lambda \bar{\Lambda} \eta$ and $\psi' \rightarrow \Lambda \bar{\Lambda} \eta$ and to validate the phase-space assumption that was used in the MC simulations, we have performed a Dalitz plot analysis of the invariant masses involved in the three-

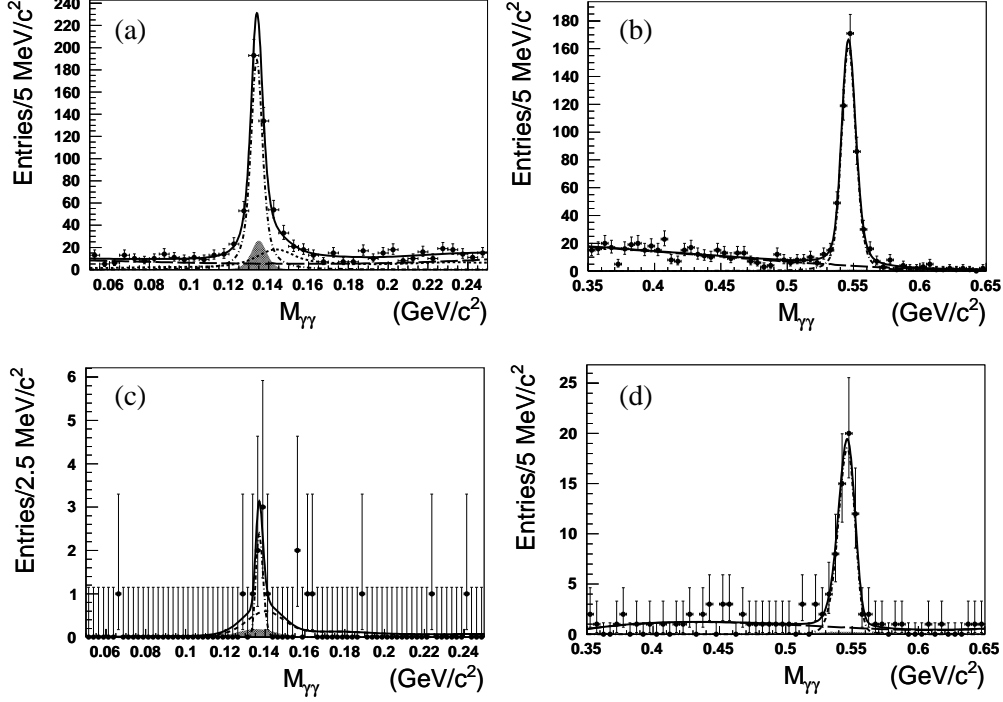


FIG. 5: The two-photon invariant-mass, $M_{\gamma\gamma}$, distributions in the π^0 and η mass regions for the channels (a) $J/\psi \rightarrow \Lambda\bar{\Lambda}\pi^0$, (b) $J/\psi \rightarrow \Lambda\bar{\Lambda}\eta$, (c) $\psi' \rightarrow \Lambda\bar{\Lambda}\pi^0$, and (d) $\psi' \rightarrow \Lambda\bar{\Lambda}\eta$. Dots with error bars are data. The solid lines are the fit to data, and the dot-dashed lines are the signal shape determined from MC simulations. The hatched histograms are the background contributions obtained from a normalized sideband analysis. The dashed lines in J/ψ , $\psi \rightarrow \Lambda\bar{\Lambda}\pi^0$ correspond to the peaking background from $\Sigma^0\pi^0\bar{\Lambda}$. The long dashed lines denote other background contributions which are described by Chebychev polynomials.

body decay. These results are shown in Fig. 6. For these plots, π^0 and η candidates are selected within mass windows of $0.12 \text{ GeV}/c^2 < M_{\gamma\gamma} < 0.14 \text{ GeV}/c^2$ and $0.532 \text{ GeV}/c^2 < M_{\gamma\gamma} < 0.562 \text{ GeV}/c^2$, respectively. In all the Dalitz plots, no clear structures are observed. A χ^2 test is performed to confirm the consistency between data and the phase-space distributed MC events. The χ^2 is determined as follows:

$$\chi^2 = \sum_i \frac{(n_i^{data} - n_i^{MC}/g)^2}{n_i^{data}},$$

where g is the scaling factor between data and MC ($g = \frac{n_{MC}}{n_{data}}$), $n_i^{data/MC}$ refers to the number of data/MC events in a particular bin in the Dalitz plot, and the sum runs over all bins. We divide the Dalitz plots into 8 bins. Boxes with very few events are combined into an adjacent bin. The $\chi^2/\text{n.d.f.}$ are equal to 1.1 and 2.1 for $J/\psi \rightarrow \Lambda\bar{\Lambda}\pi^0$ and $J/\psi \rightarrow \Lambda\bar{\Lambda}\eta$, respectively, which validates the usage of a phase-space assumption in the MC simulations.

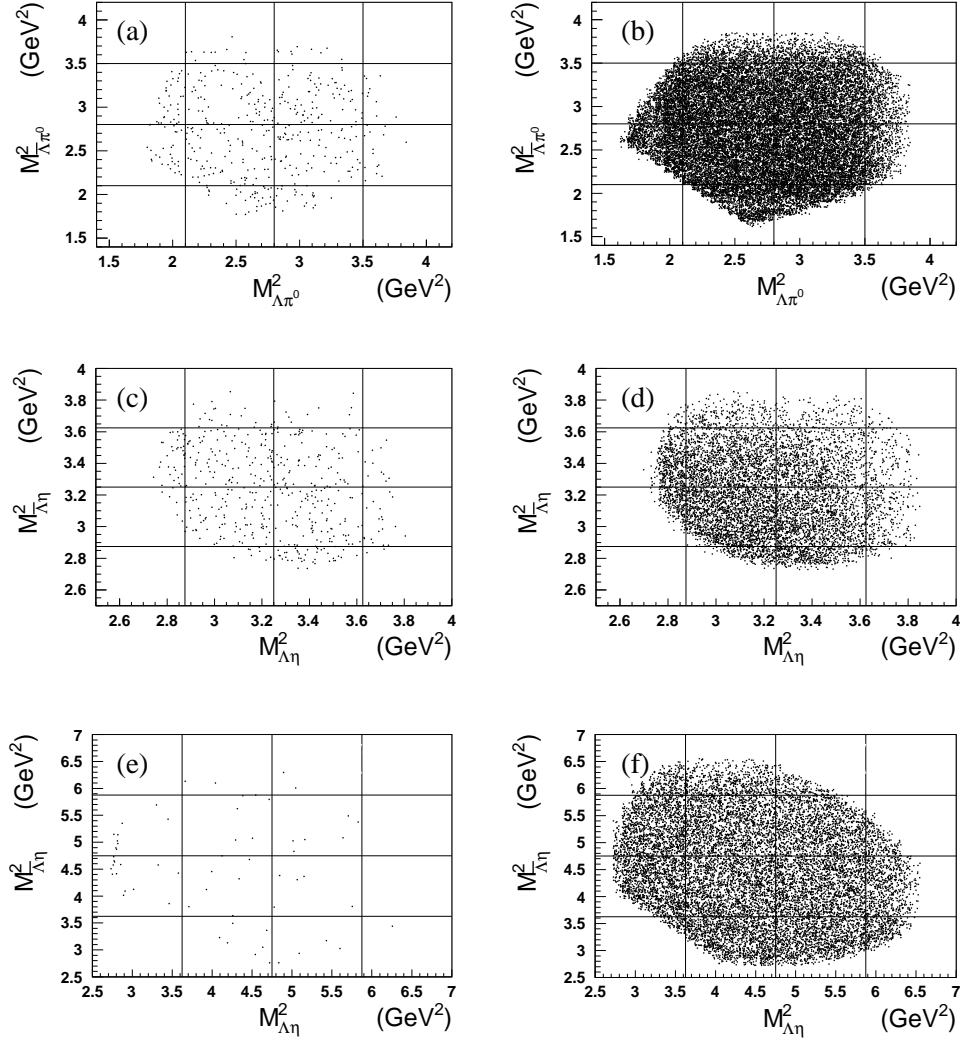


FIG. 6: Dalitz plots of the invariant masses $M_{\Lambda\pi^0(\eta)}^2$ versus $M_{\Lambda\pi^0(\eta)}^2$ for the channels (a) $J/\psi \rightarrow \Lambda\bar{\Lambda}\pi^0$ (data), (b) $J/\psi \rightarrow \Lambda\bar{\Lambda}\pi^0$ (MC), (c) $J/\psi \rightarrow \Lambda\bar{\Lambda}\eta$ (data), (d) $J/\psi \rightarrow \Lambda\bar{\Lambda}\eta$ (MC), (e) $\psi' \rightarrow \Lambda\bar{\Lambda}\eta$ (data), and (f) $\psi' \rightarrow \Lambda\bar{\Lambda}\eta$ (MC). See text for more details.

We have studied the branching fraction of the decay $J/\psi \rightarrow \Sigma(1385)^0\bar{\Lambda} + c.c.$ by combining and analyzing the invariant-mass spectra of $\Lambda\pi^0$ and $\bar{\Lambda}\pi^0$ pairs as depicted in Fig. 7. For this analysis, π^0 events are selected by applying a two-photon invariant-mass selection of $0.12 \text{ GeV}/c^2 < M_{\gamma\gamma} < 0.14 \text{ GeV}/c^2$. For the fit, the signal function is taken from a MC simulation of $J/\psi \rightarrow \Sigma(1385)^0\bar{\Lambda} + c.c.$, and the background function is taken from a MC simulation of $J/\psi \rightarrow \Lambda\bar{\Lambda}\pi^0$. A Bayesian analysis gives an upper limit on the number of $\Sigma(1385)^0\bar{\Lambda} + c.c.$ events of 37 at the 90% C.L..

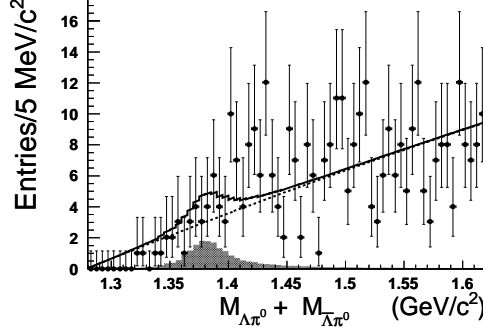


FIG. 7: A search for $\Sigma(1385)^0$ events by fitting the combined $M_{\bar{\Lambda}\pi^0}$ and $M_{\Lambda\pi^0}$ invariant-mass distributions. Dots with error bars are data. The solid line is the fit to data. The hatched histogram is the signal function obtained from a MC simulation, and the dashed line is the background function obtained from a MC simulation of $J/\psi \rightarrow \Lambda\bar{\Lambda}\pi^0$.

VI. SYSTEMATIC ERRORS

To estimate the systematic errors in the measured branching fractions of the channels of interest, we include uncertainties in the efficiency determination of charged and photon tracks, in the vertex and 4C kinematic fits, in the selection criteria for the signal and sideband region, and in the fit range. The uncertainties in the total number of J/ψ and ψ' events and in the branching fractions of intermediate state are considered as well. Below we discuss briefly the analysis that is used to determine the various sources of systematic uncertainties.

- **Tracking efficiency.** We estimate this type of systematic uncertainty by taking the difference between the tracking efficiency obtained via a control channel from data with the efficiency obtained from MC simulations. The control sample $J/\psi \rightarrow pK^-\bar{\Lambda} + c.c.$ is employed to study the systematic error of the tracking efficiency from the Λ ($\bar{\Lambda}$) decay. For example, to determine the tracking efficiency of the π^+ tracks, we select events with at least three charged tracks, the proton, kaon and anti-proton. The total number of π^+ tracks, $N_{\pi^+}^0$, can be determined by fitting the recoiling mass distribution of the $pK^-\bar{p}$ system, $M_{recoil}^{pK^-\bar{p}}$. In addition, one obtains the number of detected π^+ tracks, $N_{\pi^+}^1$, by fitting $M_{recoil}^{pK^-\bar{p}}$, after requiring all four charged tracks be reconstructed. The π^+ tracking efficiency is simply $\epsilon_{\pi^+} = \frac{N_{\pi^+}^1}{N_{\pi^+}^0}$. Similarly, we obtained the tracking efficiencies for π^- , p , and \bar{p} . With 225×10^6 inclusive MC events, we obtained the corresponding tracking efficiency for the MC simulation. The tracking efficiency difference between data and MC simulation is about

1.0% for each pion track. This difference is also about 1.0% for a proton (anti-proton) if its transverse momentum, P_t , is larger than 0.3 GeV/c. The difference increases to about 10% for the range 0.2 GeV/c < P_t < 0.3 GeV/c. Conservatively, we take a systematic error due to tracking of 1% for each pion. For the proton (anti-proton), we use weighted systematic errors, namely 2% in $J/\psi \rightarrow \Lambda \bar{\Lambda} \pi^0$, 3.5% in $J/\psi \rightarrow \Lambda \bar{\Lambda} \eta$, 1.5% in $\psi' \rightarrow \Lambda \bar{\Lambda} \pi^0$, and 2% in $\psi' \rightarrow \Lambda \bar{\Lambda} \eta$.

- **Vertex fit.** The uncertainties due to the Λ and $\bar{\Lambda}$ vertex fits are determined to be 1.0% for each by using the same control samples and a similar procedure as described for the tracking efficiency.
- **Photon efficiency.** The photon detection efficiency was studied by comparing the photon efficiency between MC simulation and the control sample $J/\psi \rightarrow \rho^0 \pi^0$. The relative efficiency difference is about 1% for each photon [16], which value was used as a systematic uncertainty.
- **Efficiency of the kinematic fit.** The control sample of $J/\psi \rightarrow \Sigma^0 \bar{\Sigma}^0, \Sigma^0 (\bar{\Sigma}^0) \rightarrow \gamma \Lambda (\bar{\Lambda})$ is used to study the efficiency of the 4C kinematic fit since its final state is the same as our signal. The event selection criteria for charged tracks and photons and the reconstruction of $\Lambda (\bar{\Lambda})$ are the same as in our analysis. If there are more than two photon candidates in an event, we loop over all possible combinations and keep the one with the smallest value for $(M_{\gamma\Lambda} - M_{\Sigma^0})^2 + (M_{\gamma\bar{\Lambda}} - M_{\bar{\Sigma}^0})^2$. Furthermore, the remaining backgrounds are suppressed by limiting the momentum windows of Σ^0 and $\bar{\Sigma}^0$, i.e., $|P_{\Sigma^0} - 980| < 40$ MeV/c and $|P_{\bar{\Sigma}^0} - 980| < 40$ MeV/c. Figure 8 shows the scatter plot of $M_{\gamma\Lambda}$ versus $M_{\gamma\bar{\Lambda}}$ for the inclusive MC events and J/ψ data after applying all event selection criteria. The square in the center with a width of 10 MeV/c² is taken as the signal region. Almost no background is found according to the topology analysis from inclusive MC events. The candidate signal events for both data and MC events are subjected to the same 4C kinematic fit as that in our analysis. The efficiency of the 4C kinematic fit is defined as the ratio of the number of signal events with and without a 4C kinematic fit. A correction factor, f_{4C} , can be obtained by comparing the efficiency of the 4C kinematic fit between data and MC simulation. i.e., $f_{4C} = \frac{\epsilon_{4C}^{data}}{\epsilon_{4C}^{MC}}$. The efficiency corrections corresponding to $\chi^2 < 15, 40, 70$ are $(90.3 \pm 0.8)\%$, $(97.5 \pm 0.6)\%$ and $(98.7 \pm 0.3)\%$, respectively. The errors in the efficiency corrections are

taken as a systematic uncertainty.

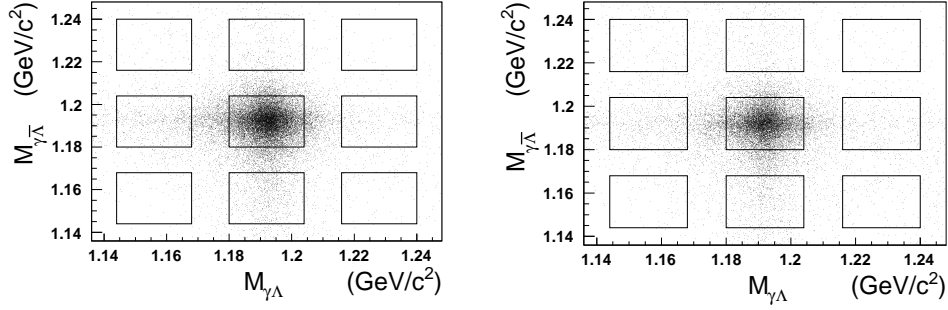


FIG. 8: The scatter plot of $M_{\gamma\Lambda}$ versus $M_{\gamma\bar{\Lambda}}$ for $J/\psi \rightarrow \Sigma^0 \bar{\Sigma}^0$ for (left) data and (right) inclusive MC events.

- Fit range. The π^0 , η , and $\Sigma(1385)^0$ yields are obtained by fitting the data around the corresponding mass value. By changing the mass ranges for the fits, the number of signal events changes slightly. These differences are taken as the errors due to the uncertainty of the fit range.
- Signal and sideband regions. By changing the signal and sideband region from $5 \text{ MeV}/c^2 \times 5 \text{ MeV}/c^2$ to $6 \text{ MeV}/c^2 \times 6 \text{ MeV}/c^2$, the number of fitted π^0 , η and $\Sigma(1385)^0$ events changes slightly for data and MC. The differences in yield between the two region sizes are taken as systematic errors.
- Background shape. A part of the background depicted in Fig. 5 is estimated by a fit with a third-order Chebychev polynomial. The differences in signal yield with a background function that is changed to a second-order polynomial, are taken as a systematic error due to the uncertainty in the description of the background shape.
- Total number of J/ψ and ψ' events. The total numbers of J/ψ and ψ' events are obtained from inclusive hadronic J/ψ and ψ' decays with uncertainties of 1.24% [4] and 0.81% [5], respectively.

All the sources of systematic errors are summarized in Table I. The total systematic error is calculated as the quadratic sum of all individual terms.

TABLE I: Systematic errors in the measurements of the branching fractions (%).

Source	$J/\psi \rightarrow \Lambda \bar{\Lambda} \pi^0$	$J/\psi \rightarrow \Lambda \bar{\Lambda} \eta$	$J/\psi \rightarrow \Sigma(1385)^0 \bar{\Lambda} + \text{c.c.}$	$\psi' \rightarrow \Lambda \bar{\Lambda} \pi^0$	$\psi' \rightarrow \Lambda \bar{\Lambda} \eta$
Photon efficiency	2.0	2.0	2.0	2.0	2.0
Tracking efficiency	6.0	9.0	4.0	5.0	6.0
Vertex fit	2.0	2.0	2.0	2.0	2.0
Correction factor of 4C fit	0.6	0.3	0.6	0.8	0.6
Background function	0.6	0.2	1.5	negligible	2.5
Signal and sidebands	3.6	1.7	negligible	9.1	2.0
Fit range	0.6	0.4	negligible	negligible	1.5
$\mathcal{B}(\Lambda \rightarrow \pi p)$	0.8	0.8	0.8	0.8	0.8
$\mathcal{B}(P \rightarrow \gamma \gamma)$	negligible	0.6	negligible	negligible	0.6
$\mathcal{B}(\Sigma(1385)^0 \rightarrow \Lambda \pi^0)$	-	-	1.7	-	-
$N_{J/\psi}$	1.24	1.24	1.24	-	-
$N_{\psi'}$	-	-	-	0.81	0.81
Total	7.8	9.7	5.6	10.9	7.6

VII. RESULTS

The branching fraction of $J/\psi (\psi') \rightarrow X$ is determined by the relation

$$\mathcal{B}(J/\psi (\psi') \rightarrow X) = \frac{N^{obs}[J/\psi (\psi') \rightarrow X \rightarrow Y]}{N_{J/\psi (\psi')} \cdot \mathcal{B}(X \rightarrow Y) \cdot \epsilon[J/\psi (\psi') \rightarrow X \rightarrow Y] \cdot f_{4C}},$$

and if the signal is not significant, the corresponding upper limit of the branching fraction is obtained by

$$\mathcal{B}(J/\psi (\psi') \rightarrow X) < \frac{N_{UL}^{obs}[J/\psi (\psi') \rightarrow X \rightarrow Y]}{N_{J/\psi (\psi')} \cdot \mathcal{B}(X \rightarrow Y) \cdot \epsilon[J/\psi (\psi') \rightarrow X \rightarrow Y] \cdot f_{4C} \cdot (1.0 - \sigma_{sys})},$$

where, N^{obs} is the number of observed signal events or its upper limit N_{UL}^{obs} , Y is the final state, X is the intermediate state, ϵ is the detection efficiency, and $\sigma_{sys.}$ is the systematic error. The branching fraction of $X \rightarrow Y$ is taken from the PDG [12]. Table II lists the various numbers that were used in the calculation of the branching fractions. With these, we obtain

TABLE II: Numbers used in the calculations of the branching fractions.

Channel	$J/\psi \rightarrow \Lambda \bar{\Lambda} \pi^0$	$J/\psi \rightarrow \Lambda \bar{\Lambda} \eta$	$J/\psi \rightarrow \Sigma(1385)^0 \bar{\Lambda} + c.c.$	$\psi' \rightarrow \Lambda \bar{\Lambda} \pi^0$	$\psi' \rightarrow \Lambda \bar{\Lambda} \eta$
Number of events N^{obs}/N_{UL}^{obs}	323	454	< 37	< 9	60.4
Efficiency ϵ (%)	9.65	8.10	6.22	8.95	14.64
f_{4C} (%)	97.5	98.7	97.5	90.3	97.5
$N_{J/\psi} (\times 10^6)$	225.3	225.3	225.3	-	-
$N_{\psi'} (\times 10^6)$	-	-	-	106.41	106.41
$\mathcal{B}(\Lambda \rightarrow \pi p)$ (%)	63.9	63.9	63.9	63.9	63.9
$\mathcal{B}(\Sigma(1385)^0 \rightarrow \Lambda \pi^0)$ (%)	-	-	87.5	-	-
$\mathcal{B}(\pi^0, \eta \rightarrow \gamma\gamma)$ (%)	98.8	39.4	98.8	98.8	39.4

$$\mathcal{B}(J/\psi \rightarrow \Lambda \bar{\Lambda} \pi^0) = (3.78 \pm 0.27 \text{ (stat.)} \pm 0.29 \text{ (sys.)}) \times 10^{-5},$$

$$\mathcal{B}(\psi' \rightarrow \Lambda \bar{\Lambda} \pi^0) < 0.29 \times 10^{-5},$$

$$\mathcal{B}(J/\psi \rightarrow \Lambda \bar{\Lambda} \eta) = (15.7 \pm 0.79 \text{ (stat.)} \pm 1.52 \text{ (sys.)}) \times 10^{-5},$$

$$\mathcal{B}(\psi' \rightarrow \Lambda \bar{\Lambda} \eta) = (2.47 \pm 0.34 \text{ (stat.)} \pm 0.19 \text{ (sys.)}) \times 10^{-5},$$

$$\mathcal{B}(J/\psi \rightarrow \Sigma(1385)^0 \bar{\Lambda} + c.c.) < 0.81 \times 10^{-5}.$$

Here the upper limits correspond to the 90% C.L..

With these results, one can test whether the branching ratio between the ψ' and J/ψ decays to the same hadronic final state, Q_h , is compatible with the expected 12% rule [6]. We find a Q_h for the channels $\Lambda \bar{\Lambda} \pi^0$ and $\Lambda \bar{\Lambda} \eta$ of

$$Q_h = \frac{\mathcal{B}(\psi' \rightarrow \Lambda \bar{\Lambda} \pi^0)}{\mathcal{B}(J/\psi \rightarrow \Lambda \bar{\Lambda} \pi^0)} < 10.0\%$$

at the 90% C.L., and,

$$Q_h = \frac{\mathcal{B}(\psi' \rightarrow \Lambda \bar{\Lambda} \eta)}{\mathcal{B}(J/\psi \rightarrow \Lambda \bar{\Lambda} \eta)} = (15.7 \pm 2.9)\%.$$

The errors reflect a quadratic sum of the systematic and statistical error, whereby some of the common sources of systematic errors have been canceled. Clearly, the isospin-violated decay $\Lambda \bar{\Lambda} \pi^0$ is suppressed in ψ' decays, while Q_h for the isospin-allowed decay, $\Lambda \bar{\Lambda} \eta$, agrees with the “12%” rule within about 1σ .

VIII. SUMMARY

This paper presents measurements of the branching fractions of the isospin-violating and isospin-conserving decays of the J/ψ and ψ' into $\Lambda\bar{\Lambda}\pi^0$ and $\Lambda\bar{\Lambda}\eta$, respectively. The results together with the measurements from previous experiments are summarized in Table III. We note that the earlier measurements of the branching fraction of the decay $\Lambda\bar{\Lambda}\pi^0$ by BES I and DM2 likely overlooked a sizeable background contribution in their analysis as supported by the BES II and BES III results. Hence, we claim that we have observed for the first time the two processes, $J/\psi \rightarrow \Lambda\bar{\Lambda}\pi^0$ and $\psi' \rightarrow \Lambda\bar{\Lambda}\eta$. Moreover, the branching fractions of the $J/\psi \rightarrow \Lambda\bar{\Lambda}\eta$ decay is measured with a drastically improved precision. Its central value is lower than the BES II measurement by about 1.5σ . The branching ratios of $J/\psi \rightarrow \Lambda\bar{\Lambda}\pi^0$ and $\psi' \rightarrow \Lambda\bar{\Lambda}\eta$ are consistent with previous upper limits, and the upper limit of $\psi' \rightarrow \Lambda\bar{\Lambda}\pi^0$ is significantly more stringent than the BES II measurement. The isospin-violating decay modes, $J/\psi \rightarrow \Lambda\bar{\Lambda}\pi^0$ and $\psi' \rightarrow \Lambda\bar{\Lambda}\pi^0$, are suppressed relative to the corresponding isospin-conserving decay modes into $\Lambda\bar{\Lambda}\eta$, albeit only by a factor of 4 in the case of the J/ψ decay. In addition, we search for the isospin violating decays of $J/\psi \rightarrow \Sigma(1385)^0\bar{\Lambda} + c.c.$ and no significant signal is observed.

TABLE III: A comparison of the branching fractions of this work with the results of previous experiments ($\times 10^{-5}$). The first error is statistical and the second one indicates the systematical uncertainty.

Experiments	$\mathcal{B}(J/\psi \rightarrow \Lambda\bar{\Lambda}\pi^0)$	$\mathcal{B}(J/\psi \rightarrow \Lambda\bar{\Lambda}\eta)$	$\mathcal{B}(\psi' \rightarrow \Lambda\bar{\Lambda}\pi^0)$	$\mathcal{B}(\psi' \rightarrow \Lambda\bar{\Lambda}\eta)$
This experiment	$3.78 \pm 0.27 \pm 0.29$	$15.7 \pm 0.79 \pm 1.52$	< 0.29	$2.47 \pm 0.34 \pm 0.19$
BES II [3]	< 6.4	$26.2 \pm 6.0 \pm 4.4$	< 4.9	< 12
BES I [2]	$23.0 \pm 7.0 \pm 8.0$			
DM2 [1]	$22.0 \pm 5.0 \pm 5.0$			

IX. ACKNOWLEDGMENT

The BES III collaboration thanks the staff of BEPC II and the computing center for their hard efforts. This work is supported in part by the Ministry of Science and Technology of China under Contract No. 2009CB825200; National Natural Science Foundation of China (NSFC) under

Contracts Nos. 10625524, 10821063, 10825524, 10835001, 10935007, 11125525, 10975143, 11079027, 11079023; Joint Funds of the National Natural Science Foundation of China under Contracts Nos. 11079008, 11179007; the Chinese Academy of Sciences (CAS) Large-Scale Scientific Facility Program; CAS under Contracts Nos. KJCX2-YW-N29, KJCX2-YW-N45; 100 Talents Program of CAS; Istituto Nazionale di Fisica Nucleare, Italy; Ministry of Development of Turkey under Contract No. DPT2006K-120470; U. S. Department of Energy under Contracts Nos. DE-FG02-04ER41291, DE-FG02-91ER40682, DE-FG02-94ER40823; U.S. National Science Foundation; University of Groningen (RuG) and the Helmholtzzentrum fuer Schwerionenforschung GmbH (GSI), Darmstadt; WCU Program of National Research Foundation of Korea under Contract No. R32-2008-000-10155-0.

-
- [1] P. Henrard *et al.* (DM2 Collaboration), Nucl. Phys. B **292**, 670 (1987).
 - [2] J. Z. Bai *et al.* (BES Collaboration), Phys. Lett. B **424**, 213 (1998).
 - [3] M. Ablikim *et al.* (BES Collaboration), Phys. Rev. D **76**, 092003 (2007).
 - [4] M. Ablikim *et al.* (BESIII Collaboration), Chinese Physics C **36**, 915 (2012).
 - [5] M. Ablikim *et al.* (BESIII Collaboration), arXiv:1209.6199.
 - [6] W. S. Hou and A. Soni, Phys. Rev. Lett. **50**, 569 (1983); G. Karl and W. Roberts, Phys. Lett. B **144**, 243 (1984); S. J. Brodsky, G. P. Lepage and S. F. Tuan, Phys. Rev. Lett. **59**, 621 (1987); M. Chaichian *et al.*, Nucl. Phys. B **323**, 75 (1989); S. S. Pinsky, Phys. Lett. B **236**, 479 (1990).
 - [7] M. Ablikim *et al.* (BESIII Collaboration), Nucl. Instrum. Methods Phys. Res., Sect. A **614**, 345 (2010).
 - [8] S. Agostinelli *et al.* (GEANT4 Collaboration), Nucl. Instrum. Meth. A **506**, 250 (2003).
 - [9] J. Allison *et al.*, IEEE Trans. Nucl. Sci. **53**, 270 (2006).
 - [10] S. Jadach, B. F. L. Ward and Z. Was, Comp. Phys. Commu. **130**, 260 (2000); S. Jadach, B. F. L. Ward and Z. Was, Phys. Rev. D **63**, 113009 (2001).
 - [11] D. J. Lange, Nucl. Instrum. Meth. A **462**, 152 (2001).
 - [12] K. Nakamura *et al.* (Particle Data Group Collaboration), J. Phys. G **37**, 075021 (2010).
 - [13] R. Ping *et al.*, Chinese Physics C **32**, 599 (2008).
 - [14] M. Xu *et al.*, Chinese Physics C **33**, 428 (2009).
 - [15] Y. S. Zhu *et al.*, Chinese Physics C **32**, 363 (2008).
 - [16] M. Ablikim *et al.* (BESIII Collaboration), Phys. Rev. D **83**, 112005 (2011).